Influence of Heat Treatment on the Mechanical Properties and Damage Development in a SiC/Ti-15-3 MMC

David A. Miller and Dimitris C. Lagoudas

Center for Mechanics of Composites
Department of Aerospace Engineering
Texas A&M University
College Station, TX 77843-3141

ABSTRACT

Titanium alloys are commonly heat-treated to meet specific design requirements. In an effort to possibly create a better composite, the influence of heat treatments on the damage evolution and strength of a SiC/Ti metal matrix composite (MMC) was studied. Heat treatments of 450°C and 700°C for 24 hours were performed on axial and transverse unidirectional specimens. These specimens, in addition to specimens in the as-received condition, were tested under non-proportional loading paths and then microstructurally analyzed to determine the induced damage state. It has been found that different heat treatments effected the elastic modulus and the macroscopic yield stress, as well as the stiffness reduction due to damage evolution. The axial composite with a 24-hr. heat treatment at 450 °C showed the highest elastic modulus and the lowest stiffness reduction than the other heat treatment conditions. The transverse composite in the as-received condition showed the highest room temperature elastic modulus and a low stiffness reduction compared with other heat treatment conditions. Typical damage modes of Ti MMC's, such as fiber matrix debonding and matrix microcracking, were seen in all three microstructural conditions. A micromechanics model based on the Mori-Tanaka averaging scheme was implemented to model the combined effects of damage and plasticity.

1 Introduction

Designs for the next generation of supersonic and hypersonic aircraft as well as engine components will require advanced materials that can withstand elevated temperatures in structural applications. Metal matrix composites (MMC's) have recently undergone serious evaluation to satisfy this need because of their high strength, low weight, and elevated temperature capabilities. Titanium has been the primary matrix material considered because of its formability, high strength-to-weight ratio, and high melting temperature (1668 °C). Titanium also has the advantage that its microstructure can be altered by alloying with metals which will stabilize the α or β phase to satisfy many different design requirements.

Structural titanium MMC's are often reinforced with continuous silicon carbide (SiC) fibers fabricated through a chemical vapor deposition process. To date, the results for the SiC/Ti systems have shown severe limitations. The composite shows improved performance in the fiber direction compared with monolithic titanium, but the transverse fiber direction properties are considerably less. Residual compressive stresses have been shown (Jeong et al., 1994, Allen et al., 1994) to form on the fiber during cooldown from the manufacturing temperature. These compressive stresses also add to the overall failure strength of the interface bond leading to failure of the composite. Lagoudas et al. (1995) studied the effect of surface damage on oxidized SiC/Ti-15-3 MMC laminates under tensile loading. An effective stiffness reduction due to the development of cracks on the surface of the composite was evaluated. Johnson (1992) has shown in composites with off axis plies that a fiber-matrix separation leads to a knee in the stress/strain curve well below the matrix yield level for a SCS-6/Ti-15-3 MMC. This damage was confirmed by a reduction in the unloading modulus and edge replicas. Replication showed fiber separation in the 90° fibers after the thermally induced compressive residual stresses had been overcome. Combined loading paths have been studied by Lissenden et al. (1995a, 1995b, and 1996), in SiC/Ti tubes. Results have shown that fiber/matrix interfacial debonding was observed in the stress-strain response and verified through microstructural evaluations.

Mujumdar and Newaz (1992a, 1992b, and 1993) have performed room temperature experimental studies of the SCS-6/Ti-15-3 composite identifying the inelastic deformation mechanisms of plasticity and damage. Newaz et al. (1992) investigated the thermal cycling response of quasi-isotropic SiC/Ti-15-3 MMC’s. Johnson et al. (Johnson et al., 1990) performed

room temperature tests to characterize the SCS-6/Ti-15-3 MMC in both the as-received condition and aged at 482°C for 16 hrs. This heat treatment was shown to increase the elastic modulus, the ultimate strength and the yield stress of the matrix.

Several different temperatures have been utilized for heat treatments in previous works, (Johnson et al., 1990, Lerch et al., 1990a) although rigorous comparisons were not made between the treatments. In fact, the motivation behind the heat treatments was not discussed, other than to stabilize the microstructure. Wolfenden et al. (1996) utilized non-destructive techniques to investigate the effect of heat treatments on the elastic modulus, damping and microhardness for SiC/Ti-15-3. The heat treatments have no documented effect on the fibers, except when performed in air at higher temperatures. The heat treatment does however affect the residual thermal stress created during processing. Lerch and associates have performed many tests on the SCS-6/Ti-15-3 system (Lerch et al., 1990b; Lerch, 1991). Lerch and Saltsman (1991), advanced Johnson's room temperature results with a study of the SCS-6/Ti-15-3 MMC at 427°C. Specimens were tested as-received and with a heat treatment of 700°C for 24 hrs. An effect of heat treatment and resulting microstructures on the damage evolution of MMC's has not been addressed.

The studies mentioned above have identified shortcomings in the material and properties which must be improved to create a viable material. The objective for this work is to study possible improvements on a SiC/Ti-15-3 MMC through different heat treatments and to experimentally characterize the deformation and damage mechanisms associated with each. The effects of the heat treatment on the thermomechanical response and damage development in unidirectional axial and transverse specimens are discussed in the second section. The third section combines averaging micromechanical techniques for both damage and plasticity into an incremental formulation for the prediction of the mechanical response of the composite.

2 Experimental Results on Thermomechanical Response of SiC/Ti-15-3 with Different Heat Treatments

2.1 Material Description and Specimen Preparation

All tests in this research were performed on material manufactured by DWA Specialty Metals using the foil-fiber-foil technique. A molybdenum interweave is commonly used in SiC/Ti MMC's to maintain fiber spacing. This process was not utilized by DWA due to the propensity for matrix cracks to initiate from the molybdenum. The composite is a 4-ply unidirectional SiC/Ti 15-3 MMC with a 32% fiber volume fraction. Fig. 1 shows a cross section of the untested material.

The matrix is reinforced by SiC fibers manufactured by British Petroleum. The fibers were produced using the chemical vapor deposition (CVD) technique around a tungsten filament. The average fiber diameter was 100 μm and has a structured carbon-titanium diboride (SCTB) coating (Allen et al., 1994).

Titanium is an allotropic material containing a lower temperature hexagonal close-packed (HCP) α-phase and a higher temperature body-centered cubic (BCC) β-phase. The alloy utilized in this composite is commonly referred to as Ti 15-3. It has an actual weight percent of 15% V, 3% Al, 3% Cr, 3% Sn and the balance Ti. Ti 15-3 is a metastable β-alloy that can completely retain the β-phase at room temperature with appropriate cooling rates. The manufacturer states the β-transus temperature for this alloy to be between 740°C and 768°C. Heat treating the alloy precipitates the α-phase throughout the β-grains and provides the dominant age-hardening mechanisms in the temperature range of 300 to 600°C (Okada, 1984). The strengthening response and ductility of different treatments varies depending on the size and volume fraction of α-precipitants.

The composite was tested in the as-received condition and with heat treatments of 450°C for 24 hr and 700°C for 24 hr. Heat treatments were performed in a vacuum to prevent oxidation from degrading the material. The as-received material contains large α-needles and dark blotchy areas known as β-prime phases. Beta prime is a solute lean, BCC phase that appears to develop where α precipitation is sluggish, labeled as B in Fig. 1. The α-particles, labeled as A in Fig. 1, are seen primarily along the fiber interface creating a β-depleted zone around the fiber area. The α rich region surrounding the fiber is opposite to the characteristics

seen in the SCS-6/Ti-15-3 systems. These have been shown (Lerch and Saltsman, 1991) to have precipitant lean zones around the fibers. It is possible that the amount of precipitation is due to the diffusion of the fiber coating into the matrix, since carbon is an α-stabilizer and silicon is a β-stabilizer. This possibility was studied by examining the chemical concentrations across the interface. Fig. 2a shows a typical fiber-matrix interface region from which an energy dispersive spectroscopy (EDS) line scan was taken, the line scan moved from point 1 to point 2 on the photograph. Fig. 2b shows the results of the line scan profile illustrating the variation of silicon and carbon concentration across the interface. The plot shows that the silicon concentration drops as the profile moves from the fiber region to the titanium, and returns to same level as the scan moves back into the fiber. The carbon concentration shows a dramatic spike at the point where the silicon level drops. A very large interface region is seen in the photograph, which seems to be the location of the carbon rich region. The fiber coating differs for the Sigma fiber and SCS-6 fiber, therefore the possibility of different interfaces exists.

The 450°C heat treatment produces a small fine α-particle precipitant with virtually no congregation along the grain boundary, as seen in Fig. 3. It has been shown (Lerch et al., 1990a) that this heat treatment produces the highest room temperature modulus for the matrix material. This is expected since the HCP α-phase has a higher stiffness than the BCC β-phase. However, the increase in α-phase also removes the slip planes of the BCC β-phase and causes a severe drop in the ductility of the material. The distinct interface region remains, but the precipitant accumulation around the fiber has disappeared. The aging has caused the precipitant to distribute throughout the grain structure. Grain boundaries are still the same size, but not as apparent as before the redistribution.

The 700°C for 24hr heat treatment, Fig. 4, creates large α-needles dispersed throughout the β-phase grains, and the grain size remains unchanged. The β-depleted region around the fibers is still present, as well as the grain boundary phases. It has been shown that this heat treatment slightly reduces the stiffness of the titanium (Lerch et al., 1990a) from the as-received condition, but the ductility increases substantially. The microstructure for this treatment is very stable after long exposures at elevated temperatures.

2.2 Thermomechanical Testing Description

All tests were performed on an MTS servo-hydraulic load frame under load control at a rate of 10.4 MPa/sec. Elevated temperature tests were performed using a three-zone clamshell

resistance furnace. Three temperature controllers monitored the specimen temperature from thermocouples spot-welded to the specimen at the top, middle and bottom of the gage section. The controllers were able to maintain, and all tests were performed within, ±3°C of the set temperature. Strain measurements for all tests were made with a one-inch gage high temperature extensometer.

Three different mechanical loading paths were used to study the development of inelastic deformation in the composite. These loading paths were performed at room temperature and at 427°C (800°F) for each of the heat treatments. The elevated testing temperature was selected because it is a potential operating temperature of the MMC. A monotonic tension test and two non-proportional loading tests with increasing stress amplitudes were performed. One monotonic tension test was performed at each testing temperature, using a specimen in the as-received condition, to determine the overall deformation characteristics and limits of the composite. Two types of non-proportional cyclic tension tests with increasing stress amplitudes were performed to monitor the degradation from the initial modulus. The first type of cyclic test utilized an R=0.1, and the second type of cyclic test unloaded 14 MPa from the peak stress level in each cycle. The second type of cyclic test was performed to eliminate the knee seen on the unloading curve, due to closing of the debonded fiber/matrix interface (Johnson et al., 1990), however, a shortage of specimens made these tests unavailable for every heat treatment. Limited material did not allow for multiple tests of the same heat treatment condition, and the variability of the initial elastic modulus due to manufacturing flaws cannot be addressed. However, all specimens were taken from the same composite plate, thus, the manufacturing process was identical for each specimen. Note also that the stiffness reduction is the variable correlated to damage evolution, and in all specimens tested a reduction in the stiffness has been observed. Due to the inconsistencies seen in the composite plate, and the low number of specimens tested, this study only qualitatively addresses the influence of the heat treatment on the material parameters (e.g., elastic modulus) of the composite.

Microstructural evaluations were performed after each test to determine the state of damage in the composite. The specimens were carefully sectioned using a diamond-wafering blade. An extensive polishing procedure was utilized to prepare the samples for microstructural evaluation. Specimens were etched using Kroll's reagent to reveal the microstructure and grain

boundaries. Microstructural evaluations were performed with light microscopy and scanning electron microscopy.

The following sections discuss the testing of the unidirectional composite in the axial and transverse directions at room temperature and 427 °C.

2.3 Axial Tension Tests

Room Temperature Results

Three cyclic tests, one for each heat treatment condition, were conducted at room temperature. Fig. 5 shows the stress-strain response for the room temperature tests. A significant feature of this plot is the differences in the response of the 450°C heat treatment specimen from the response other the heat treatments. This test specimen shows no significant yielding before failure and has a higher elastic modulus than the specimens subjected to the other heat treatments. The as-received specimen has the lowest elastic modulus of the three treatments, although the 700°C specimen is only slightly higher. The unloading elastic modulus from each cycle is plotted in Fig. 7 with the total applied stress from that cycle for each heat treatment. A loss in elastic unloading stiffness indicates that damage has been introduced into the specimen, and as seen in Fig. 7, a reduction in elastic modulus is seen for each specimen as the loading stress increases. The 450°C specimen shows an initial damage growth which appears to saturate with the overall applied stress to a level which no further damage occurs. The remaining two heat treatments show a continuous damage evolution with no apparent saturation state.

Elevated Temperature Results

Fig. 6 shows the stress vs. strain plots for the three axial specimens tested at 427 °C. The plots show, similar to the room temperature results, that the 450°C specimen has the highest modulus and the highest yield point. Analysis of the unloading modulus, Fig. 7, shows that the 450°C specimen has a high initial elastic modulus that decreases 13% after the first cycle. However, unlike the room temperature tests, the damage state does not saturate, and damage continues to accumulate as the stress level increases. Fig. 6 also shows that plastic strains begin to accumulate for the 450°C specimen at 600 MPa. Damage steadily grows in the as-received and 700°C specimens indicated by the continuous reduction in unloading modulus with increasing applied stress, Fig. 7, similar to that seen in the room temperature tests.

Axial Tension Discussion

The above axial tension tests showed that the heat treatments affected the mechanical response of the composite in the axial fiber composite. For both the room temperature and elevated temperature tests, the 450°C heat-treated specimens had a higher modulus and yield point than the other two treatments. This was expected since the 450 °C heat treatment creates the highest room temperature modulus and yield point in the matrix due to the high concentration of HCP α-phase seen throughout the matrix. The inelastic deformation in the axial direction has been shown to be primarily dominated by matrix plasticity, rather than damage (Majumdar and Newaz, 1992a). Regardless of the heat treatment and testing temperature, all specimens failed in the range of the fiber strain limit of 0.9-1.0%.

The as-received and 700°C heat-treated specimens showed similar results for both temperatures. They share similar microstructures with the primary difference being the size of the precipitant, see Figs. 1 and 4. It is interesting to note the increase of the elevated temperature elastic modulus to a value above that observed for the room temperature elastic modulus (Figs. 5 and 6). This observation may be explained by the manufacturing inconsistencies that exist from specimen to specimen. Microstructural evaluation of the specimens reveals both fiber cracks and matrix cracks in room and elevated temperature tests. Fig. 8 shows cracks developing perpendicular to the fiber, or loading, direction and the etched specimen reveals the crack growth along the α-rich grain boundary for the as-received specimen. The saturation to constant modulus seen by the 450 °C heat treatment tested at room temperature is consistent with this microstructural analysis due to the absence of grain boundary α-precipitants. As matrix cracks extend to the fiber, debonding occurs and load sheds to the fiber. Microscopic evaluation showed that the fiber/matrix interface was debonded on failed specimens. From the catastrophic failure seen and heard when the composite failed, it can be assumed that the fibers fail almost simultaneously.

Fig. 7 shows the unloading modulus for both the room and elevated temperature axial specimens as a function of the applied load. The figure shows that the damage accumulation at elevated temperatures, identified by the decrease in elastic modulus, increases throughout the test without saturating to a constant value. The continuous damage accumulation with increasing load could be explained by the decrease in the compressive thermal residual hoop stress around the fiber at elevated temperatures. As the residual stresses decrease, the

mechanically applied stress overcomes the compressive stress and the critical strength of the interface is reached at a lower stress level creating a fiber/matrix interface crack and a loss of stiffness.

2.4 Transverse Tension Tests

Room Temperature Results

Tension tests of unidirectional transverse fiber specimens showed that the heat treatment increased the ductility of the composite by 0.1% from the as-received condition. This increase is almost negligible since the failure strain of unreinforced Ti 15-3 can reach approximately 12% strain (Lerch et al., 1990a), two orders of magnitude greater than the 0.3% failure strain under transverse loading of the composite. The low failure strain can be attributed to the pre-existing flaws seen in the material, which result in premature damage and failure. The initial modulus measured in monotonic tests closely matches published results for similar systems (Mujumdar and Newaz, 1992a), although ultimate tensile strength (UTS) and failure strain remain well below previous results. Published works on other Ti-15-3 MMCs utilize an SCS-6/Ti-15-3 composite from another manufacturer. Observations similar to those presented here have not been reported in the literature, but microstructural evaluations suggest a correlation between failure strain and the voids that are present in the specimens tested in this work which are apparently formed during consolidation.

A total of five non-proportional loading tests were performed on specimens at room temperature. Fig. 9 shows a stress vs. strain response for each heat treatment. Microstructural evaluations were performed on the specimens to study the damage modes. Tests with large unloading cycles show two distinct linear regions, which has been noted in earlier works by Mujumdar and Newaz, (1992b) and described as a knee in the curve. It has been suggested that this is due to the closing of circumferential cracks, thus engaging a frictional force which increases the unloading elastic modulus the material. Reloading the specimen shows a higher elastic modulus than seen on the unloading curve, thus generating a hysteresis effect upon reloading. As seen in Fig. 9, the hysteresis effect is more prominent at larger stress levels. The as-received and 700°C specimens showed little permanent deformation, therefore the inelastic deformation is attributed mostly to damage.

Elevated Temperature Tests

The as-received, 450°C and 700°C specimens failed at 242 MPa (35 ksi), 274 MPa (39.7 ksi) and 244 MPa (35.4 ksi) respectively. Five non-proportional tests were performed and the results for each heat treatment are shown in Fig. 10. The as-received specimen has a significantly different elastic modulus from the room-temperature tests, however, the permanent strain is similar to the room-temperature tests. The characteristic knee in the unloading curve is still present in the early cycles, but is not evident in the later cycles at higher stress levels, although the hysteresis effect is observed in all the specimens and is larger than in the room-temperature hysteresis. Fig. 11 shows the unloading modulus for each of these tests. The 700°C heat treatment is the only treatment that shows a dramatic drop in the unloading modulus. This specimen failed at a stress level below that of the monotonic tension test, suggesting that the specimen had a dominant flaw that deteriorated the material strength quickly resulting in premature failure. A sharp drop is seen at the end of the 450 °C heat treatment curve suggesting that a critical stress level for damage growth was reached. The remaining plots show that the rate of damage development, seen through a loss of stiffness, is comparable for each heat treatment.

Transverse Tension Discussion

Specimens with identical heat treatments showed different mechanical responses from test to test, making conclusions difficult to make. For the room temperature tests, the as-received specimen showed the highest initial modulus, but damage quickly reduced the modulus as higher load levels were reached. The effect of the heat treatment on the transverse composite stiffness is inconsistent with the results from the axial tension tests, as will be discussed later this may be explained by the resulting damage evolution. The 450°C specimen had the lowest modulus at room temperature and showed the greatest rate of stiffness loss, which is opposite from the axial fiber specimens. As seen in Fig. 11, the 700°C specimen tested at 427 °C had the highest modulus, but also showed the greatest loss of stiffness, while the 450°C and as-received specimens, at the same temperature, showed very similar responses for the rate of stiffness loss. The 700 °C specimen showed the highest rate of stiffness loss, however the resulting stiffness never decreased below that of the other specimens. This point could be explained by the

accumulation of microcracks reaching a saturation point at which the modulus no longer changes. The results of the room temperature unloading modulus also support the conclusion that damage evolution tends to saturate to a constant damaged state.

Microstructural evaluation shows that damage for all of the specimens primarily occurs in the form of interface debonding and matrix cracking. Microphotographs of the damage induced during the monotonic tests for a typical as-received specimen shows cracks emanating from the voids around the fibers. These cracks propagate and finally connect in the area between fibers. Fig. 12 shows examples of the damaged microstructure before and after it has been chemically etched. The propagation of cracks between the fibers is clearly visible in the photographs before etching. The photographs of the etched specimen reveal the grain boundaries and the cracks propagating along the boundaries separating the fibers. Such progression of cracks along grain boundaries has not been seen in previous studies. Previous studies (Newaz and Mujumdar, 1992a) have shown matrix cracks to develop from shear bands that emanate from radial cracks in the fiber matrix interface and eventually fail the composite. The present study found a slight presence of the same radial cracks, but shear banding was not present. Instead, it can be suggested, based on microphotographs of failed specimens, that final failure of the composite occurred from an accumulation of the cracks developed along the grain boundaries which eventually coalesce between the fibers. The grain boundary is prone to crack development due to the brittle α-phase that accumulates along the grain boundary. From the etched microstructures seen in figs. 1, 3, 4 and12 the highest level of α phase grain boundary accumulation is seen in the 700 °C heat treatment specimens and the lowest accumulation is seen in the 450 °C heat treatment specimens. The premature failure of the specimens and lack of large permanent deformation, as compared to similar material systems, leads to the conclusion that crack development along the grain boundary led to failure of the specimens at stress levels well below the matrix yield stress.

Results from previous studies on similar Ti-15-3 (Johnson et al., 1990, Newaz and Mujumdar, 1992a) systems show three distinct regions of deformation in the transverse composite. The first region is purely elastic, followed by a region dominated by damage growth, and the third region is dominated by matrix plasticity. The stress levels reached in the third region, for similar systems, are above the failure stresses of the composite used in this study. The lack of the third region of deformation in the present experimental results indicates that

matrix dominated deformation has not been achieved, hence, providing an explanation for the lack of shear bands present in the material.

3 Thermomechanical Modeling of Damage and Plasticity in SiC/Ti-15-3 MMC

3.1 Model Development

In this section an attempt will be made to correlate the experimental observations with theoretical modeling. The actual deformation mechanisms are complex and involve plasticity and damage evolving during the loading. An elaborate finite element model can capture the local plastic deformation and fiber/matrix interface effects, but this approach is very cumbersome and creates problems and uncertainties not seen in an averaging scheme. An approximate averaging micromechanics method will be used to model the influence of the loading direction and material properties on the mechanical response of the composite. The model will be based on the extension of the Mori-Tanaka micromechanics averaging method (Mori and Tanaka, 1973) to include damage and plasticity effects.

Averaging methods have been developed which model either incremental plasticity or damage in fibrous composites. In the present study, an attempt will be made to combine into a single model, simultaneous plasticity and damage in an incremental formulation. For the present implementation of the incremental formulation of combined plasticity and damage, the increment of total strain, $\Delta\bar{e}^{t}$, for each increment of applied overall stress, $\Delta\bar{s}$, is expressed as the sum of the elasto-plastic strain increment, and strain increment due to damage, i.e.,

$$\Delta\bar{e}^{t} = \mathbf{M}^{ep}\Big|_{\bar{s}+\Delta\bar{s}}\,\Delta\bar{s} + \left[\mathbf{M}^{d}\Big|_{\bar{s}+\Delta\bar{s}} - \mathbf{M}^{d}\Big|_{\bar{s}}\right]\bar{s}\,, \tag{1}$$

where the instantaneous elasto-plastic tangent compliance is evaluated at the end of the stress increment. The first term in the above equation describes the elasto-plastic strain increment calculated by the instantaneous compliance, $\mathbf{M}^{ep}$, and the second term calculates the strain increment introduced by damage through the change in the elastic damage compliance $\mathbf{M}^{d}$.

Solving for the total strain increment requires determination of the instantaneous elasto-plastic compliance, $\mathbf{M}^{ep}$ and instantaneous elastic compliance $\mathbf{M}^{d}$. These quantities can be determined by several methods, including FEM formulations, and averaging techniques such as the self-consistent method and the Mori-Tanaka method. Averaging techniques based on the

Eshelby solution have been extensively used to evaluate effective elastic material properties (Mura, 1982, Christensen, 1979). The Mori-Tanaka averaging method (Weng, 1984, Benveniste, 1987) has been shown to produce predictions close to numerical results in unidirectional composites undergoing inelastic deformations under monotonic loadings (Lagoudas et al., 1991). In addition to its reasonable accuracy, the convenience of using the Mori-Tanaka method, as supposed to the self-consistent method for example, becomes clear when computational time is considered, especially in the incremental formulation required for analyzing elasto-plastic response. Numerical techniques, such as FEM for periodic composites (Foulk et al., 1997), are also potential methods to solve the complex system of damage and plasticity, however, the exact incorporation of damage requires large computational effort and exact knowledge of the damage mechanisms.

The Mori-Tanaka method utilizes the Eshelby equivalence tensor, **S**, to calculate the elastic stress concentration factor, $\mathbf{B}^{e}_{n}$, which relates the overall applied stress, $\overline{s}$, to the stress in the α phase by

$$s_{\alpha} = \mathbf{B}^{e}_{\alpha}\overline{s} \quad , \qquad \alpha = \text{f, m} \tag{2}$$

where α indicates the fiber or matrix phase. For a two-phase composite, a computationally convenient stress concentration factor based on the Mori-Tanaka approximation is given by (Gavazzi and Lagoudas, 1990)

$$\mathbf{B}^{e}_{f} = [\mathbf{I} + c_{m}\,\mathbf{L}^{e}_{m}(\mathbf{I}-\mathbf{S})(\mathbf{M}^{e}_{m} - \mathbf{M}^{e}_{m})]^{-1} \tag{3}$$

where $\mathbf{L}^{e}_{a}$ and $\mathbf{M}^{e}_{a}$ are the elastic stiffness and compliance tensors respectively, c_{α} is the volume fraction for each phase and **I** is identity matrix. The elastic concentration factor $\mathbf{B}^{e}_{m}$, is calculated from the relation

$$c_{f}\,\mathbf{B}^{e}_{f} + c_{m}\,\mathbf{B}^{e}_{m} = \mathbf{I}\,. \tag{4}$$

The effective elastic compliance for the MMC can then be found using the following equation (Hill, 1965),

$$\mathbf{M}^{e} = c_{f}\,\mathbf{M}^{e}_{f}\mathbf{B}^{e}_{f} + c_{m}\,\mathbf{M}^{e}_{m}\mathbf{B}^{e}_{m}\,. \tag{5}$$

Substituting the elastic modulus for each heat treatment into the above equations yields an evaluation of effective elastic compliance for each heat treatment of the composite.

As the loading is increased, matrix cracks develop in the unidirectional composite laminate and the above evaluation of the elastic compliance must be modified to account for the developing damage. From eq. (1), the overall strain increment due to damage is given by

$$\Delta\bar{e}^{\mathrm{d}} = [\mathbf{M}^{\mathrm{d}}\big|_{\bar{s}+\Delta\bar{s}} - \mathbf{M}^{\mathrm{d}}\big|_{\bar{s}}]\bar{s} \ , \tag{6}$$

where the damage compliance, $\mathbf{M}^{\mathrm{d}}$, is a function of the overall applied stress, $\bar{s}$. Fig. 13 shows a schematic representation of a uniaxial loading and illustrates the relation between the damage compliance, $\mathbf{M}^{\mathrm{d}}$, to the overall damage strain increment, $\Delta\bar{e}^{\mathrm{d}}$. The effect of cracks on the overall compliance of the composite is modeled using the methods derived by Laws and Dvorak (1987), and Dvorak et al. (1985) which relate the composite compliance to the density of cracks in the composite. Two different types of cracks are modeled, slit-cracks in transverse fiber composites and penny-shaped matrix cracks in axial fiber composites. Using this method, cracks developed along the fiber/matrix interface are not taken into account in this model and are considered as perfectly bonded throughout the entire loading.

Cracks developed in transverse specimens are modeled as slit cracks parallel to the fiber direction extending along the length of the fiber. The crack density, β^{tr}, is a function of the overall applied stress, and is defined as the number of cracks of length, *a*, in a square cross-section of material with sides of length *a*. The Mori-Tanaka method is used to generate the elastic compliance, $\mathbf{M}^{\mathrm{e}}$, of the undamaged composite, which is then combined with the influence of the cracks to generate the effective compliance of the damaged composite, $\mathbf{M}^{\mathrm{d}}$, as a function of applied stress, using the relation

$$\mathbf{M}^{\mathrm{d}} = \mathbf{M}^{\mathrm{e}} + \frac{p}{4} b^{\mathrm{tr}} \mathbf{\Lambda}^{\mathrm{tr}} \ . \tag{7}$$

The tensor quantity, $\mathbf{\Lambda}^{tr}$**,** has only three non-zero components $\mathbf{\Lambda}^{tr}(2,2)$, $\mathbf{\Lambda}^{tr}(4,4)$ and $\mathbf{\Lambda}^{tr}(6,6)$ which are expressed in terms of the composite elastic compliance, $\mathbf{M}^{\mathrm{e}}$ (Dvorak et al., 1985).

In the axial specimens, cracks are modeled as a collection of penny-shaped cracks that bypass the fibers and extend into the matrix. The crack density, β^{a}, is a function of applied load and is defined as the average number of cracks of specific diameter, *d*, in a cube with sides of length, *d*. The effective compliance of the composite is calculated in two steps. First, the matrix

is regarded as a volume of homogenous material with similar cracks of density β^a, for which an effective compliance, $\mathbf{M}_{\mathrm{m}}^{\mathrm{d}}$, is calculated by

$$\mathbf{M}_{\mathrm{m}}^{\mathrm{d}} = \mathbf{M}_{\mathrm{m}}^{\mathrm{e}} + \frac{p}{6} b^{\mathrm{a}} \mathbf{\Lambda}^{\mathrm{a}} \ . \tag{8}$$

The tensor quantity, $\mathbf{\Lambda}^a$, has only three non-zero components, $\mathbf{\Lambda}^a(3,3)$, $\mathbf{\Lambda}^a(4,4)$, and $\mathbf{\Lambda}^a(5,5)$ which are expressed in terms of the elastic compliance of the matrix, $\mathbf{M}_{\mathrm{m}}^{\mathrm{e}}$ (Dvorak et al. 1985). The second step utilizes the Mori-Tanaka method, equations (2)-(5), to generate an effective compliance of the damaged composite, $\mathbf{M}^{\mathrm{d}}$, using the properties of the fiber and the damaged matrix, $\mathbf{M}_{\mathrm{m}}^{\mathrm{d}}$. Implementations of these models are discussed more thoroughly later in the paper.

To model the plasticity effects in the matrix, the overall elasto-plastic strain increment defined in eq. (1), or $\Delta\bar{e}^{\mathrm{ep}}$, is found using an existing method which combines the incremental plasticity equations with the Mori-Tanaka averaging scheme and is evaluated in the present implementation using a backward Euler integration scheme, i.e.

$$\Delta\bar{e}^{\mathrm{ep}} = \mathbf{M}^{\mathrm{ep}}\Big|_{\bar{s}+\Delta\bar{s}} \Delta\bar{s} \tag{9}$$

Lagoudas et al. (1991) have derived history dependent concentration factors and developed a numerical scheme for the integration of the combined system of matrix plasticity equations together with the equations that define the concentration factors, and results from this development have produced excellent results for an MMC in a singular loading direction. For a loading increment, $\Delta\bar{s}$, the relation given in equation (2) is utilized to determine the stress increment in the matrix, which is assumed to undergo plastic deformations when the yield condition is satisfied. In the presence of plastic deformation, the following system of nonlinear algebraic equations has to be solved for $\Delta s_{\mathrm{m}}, \Delta a_{\mathrm{m}}$ and Δl_{m}:

$$\Delta\boldsymbol{\sigma}_{\mathrm{m}} = \mathbf{B}_{\mathrm{m}}(\boldsymbol{\sigma}_{\mathrm{m}} + \Delta\boldsymbol{\sigma}_{\mathrm{m}}, \boldsymbol{\alpha}_{\mathrm{m}} + \Delta a_{\mathrm{m}})\Delta\bar{s}\,, \tag{10}$$

$$\Delta a_{\mathrm{m}} = \Delta l_{\mathrm{m}} n_{\mathrm{m}}(\boldsymbol{\sigma}_{\mathrm{m}} + \Delta\boldsymbol{\sigma}_{\mathrm{m}}, \boldsymbol{\alpha}_{\mathrm{m}} + \Delta a_{\mathrm{m}})\,, \tag{11}$$

$$\Phi(\boldsymbol{\sigma}_{\mathrm{m}} + \Delta\boldsymbol{\sigma}_{\mathrm{m}}, \boldsymbol{\alpha}_{\mathrm{m}} + \Delta a_{\mathrm{m}}) = 0\,, \tag{12}$$

where $\boldsymbol{\alpha}_{\mathrm{m}}$ are the kinematic hardening internal state variables and Φ is the yield criterion. Explicit evaluations are given for a Mises yield criterion and kinematic hardening according to Phillips hardening rule. An iterative method, starting with an elastic predictor, is used to solve the system of plasticity equations for increments of the state variables. The concentration factor,

$\mathbf{B}_m$, is evaluated first using the elastic material properties of both phases. This estimate is then corrected by

$$\Delta\boldsymbol{\sigma}_m^{j+1} = \mathbf{B}_m^j \Delta\bar{s}, \quad j = 1,2,\ldots \tag{13}$$

where the stress concentration factor $\mathbf{B}_m^j$ is evaluated from equations (3) and (4) using the updated plastic matrix compliance, $\mathbf{M}_m^{ep}$, i.e.

$$\mathbf{M}_m^{ep} = \left.\frac{3\mathbf{n}_m\mathbf{n}_m^T}{2H\mathbf{n}_m^T\mathbf{n}_m^*}\right|_{(s_m+\Delta s_m)} + \left.\mathbf{M}_m^d\right|_{\bar{s}+\Delta\bar{s}} \tag{14}$$

where H is the instantaneous tangent modulus, $n_m = \frac{\partial\Phi_m}{\partial\boldsymbol{\sigma}_m}$, $\sigma_m^*\big|_k = b_m g$ for k=1,2,3, and $\sigma_m^*\big|_k = b_m g/2$ for k=4,5,6. The quantity $\mathbf{M}_m^{ep}$ is then used to update the **S** tensor numerically (Gavazzi and Lagoudas, 1990). If a convergence criterion is satisfied, using the final values of the local stress increments, the resulting total strain increment, elastic and plastic, is calculated using the composite plastic compliance, $\mathbf{M}^{ep}$
where

$$\mathbf{M}^{ep} = \mathbf{M}_m^{ep} + c_f\left(\mathbf{M}_f^e - \mathbf{M}_m^{ep}\right)\mathbf{B}_f \tag{15}$$

The procedure is repeated for each new increment of stress until the entire loading path is complete.

3.2 Implementation and Comparison with Experiments

Implementation of the averaging micromechanics approach to predict the mechanical response for combined plasticity and damage requires knowledge of the elastic yield stress, the instantaneous tangent modulus for the plastic response of the matrix, and the evolution of the crack density, β, as a function of applied load. A damage growth model relating the crack density to the applied load is not utilized in this paper due to the inherent complexities those models contain. In the absence of a damage growth criterion, an experimental measurement will be utilized to determine the contribution of damage to the total inelastic deformation during a given loading path. Specifically, the damage will be determined from the experimentally measured component of the elastic unloading stiffness, $\mathbf{L}^d$, shown in Figs. 7 and 11, where

$\mathbf{L}^{d} = [\mathbf{M}^{d}]^{-1}$. A prediction of crack density as a function of applied load can be determined by solving eq. (7) for the transverse crack density, β^{tr}, and eq. (8) for the axial crack density, β^{a}, that yields the experimentally measured component of the unloading elastic stiffness. Since only uniaxial stress states are investigated, only the components of stress, strain and compliance in the loading direction will be calculated, the solution of from these equations is shown in Fig. 14 using the material properties listed in Table 1. The predicted crack density in the axial specimens, Fig. 14a, shows that damage growth with applied load in the 450°C heat treatment is two to three times greater than the damage growth for the as-received and 700°C heat treatments. The predicted crack density in the transverse specimens, Fig. 14b, also shows that damage growth with applied load in the 450°C heat treatment is greater than the damage growth for the as-received and 700°C heat treatment, however, the 700°C heat treatment tested at 427°C also showed a high damage rate.

The model is developed in such that the only material constant necessary to model the elasto-plastic response is the yield stress and the instantaneous tangent modulus, H. This method has been successfully implemented for MMCs, as mentioned, when a uniform composite is analyzed. The stress concentrations arising from the material flaws in the composite used in the present study are discussed to cause yielding of the composite at a stress level well below that of similar material systems and the matrix itself. However, in an attempt to successfully test the developed model using the experimental data, changes must be made in the approach.

Implementation of the plastic response of the composite requires only the knowledge of the plastic response of the matrix, specifically, the yield stress and the instantaneous tangent stiffness, *H*. Tensile tests on the matrix material have shown large plastic deformations with little hardening. Similar results for the transverse composite have also been seen in previous results (Mujumdar and Newaz, 1992a), however, the region of large plastic deformation occurs at stress levels well above those attained in the experiments performed in this study. The composite investigated in this study plastically deformed and failed due to the pre-existing damage, discussed in section 2, at a stress level well below the yield stress seen in similar composite systems without pre-existing damage. The effect of the local stress concentrations in the areas surrounding the pre-existing flaws is a change in the elastic matrix stress concentration factor, $\mathbf{B}_{m}^{e}$. As discussed above, this term relates the overall applied stress to the stress in the matrix and is based on the Eshelby solution. Thus, when this factor is utilized for the composite

used in this study, the elastic stress concentration factor underpredicts the stress state in the matrix. However, for implementation purposes in this study, the effect of the stress concentrations on the elastic stress concentration factor is taken into account by utilizing a lower matrix yield stress. This method was preferable over solving for a new elastic stress concentration factor due to its simplicity. Also, this method allows for successful testing of the model to combine both elasto-plastic deformation and damage through simulation of the experimental data. It must be noted that this method is not necessary for composites without such defects, and is utilized simply due to the premature yielding seen in this composite. If the material flaws did not exist in the material, the nominal values for yield stress satisfactory results for the plastic response of the material when compared with similar material systems (Mujumdar and Newaz, 1992a).

Using the results shown in Figs. 14, the overall stress vs. strain response can be simulated accounting for both elasto-plastic deformation and damage evolution. In the absence of a damage criterion, experimental results of stiffness loss with applied load are utilized to predict the crack density with increasing load. Comparison between simulated stress/strain response and experimental measurements are seen in Fig. 15a for the axial specimens and in Fig. 15b for the transverse specimens, and show the successful simulation of experiments utilizing the methods described herein. In the simulation of the transverse loading, the knee in the unloading portion of the experimental curve, explained by the engaging of frictional forces upon crack closure, is not taken into account in this model. This results in an overprediction of the damage strain at the higher stress levels where the knee becomes more pronounced. Therefore, the stress/strain simulation is not continued into higher levels of stress. To verify the model predictions for resulting crack density, β, as a function of applied load, post-test microstructural evaluations were performed. The crack densities measured from the specimens are compared to the predicted crack densities at the maximum applied stress seen in Fig. 14. Table 2 contains the measured and predicted values of the crack densities for each heat treatment and test temperature for the transverse composite. Note that for the axial specimens, identification of the crack density was not as evident as in the transverse composite. Although damage was predicted, and seen, in all axial specimens, a regular interval of cracks was not clearly observable, suggesting that the damage growth in the composite was isolated to local

areas surrounding dominant flaws. Therefore, no quantitative comparisons have been attempted between the predicted values of damage and the experimentally observed ones.

Matrix Properties						
	Room temperature			**Elevated temperature, 427**°C		
	As- Rcvd	450 °C	700 °C	As- Rcvd	450 °C	700 °C
E, GPa	92.4	104.8	90.0	78.0	83.0	77.5
ν	.32	.32	.32	.32	.32	.32

	Fiber Properties
	Room temperature and Elevated temperature
E, GPa	395.1
ν	.19

Table 1: Material Properties for each heat treatment utilized in modeling (Lerch et al., 1990a, Johnson et al., 1990, Wolfenden et al., 1996)

	Room temperature			**Elevated temperature, 427 °C**		
	As- Rcvd	450 °C	700 °C	As- Rcvd	450 °C	700 °C
Experiment	.38	.45	.48	.32	.40	.35
Prediction	.39	.60	.32	.33	.72	.66

Table 2: Comparison of Experimental and Predicted Crack Densities, β^{tr}, after final loading for transverse specimens.

In transverse specimens, the crack density was calculated as the average crack length divided by the average crack spacing measured from a microphotograph of each sample. The crack length was taken to be the width of the void around the fiber, as seen in Fig. 12. The predicted crack densities for the transverse specimens, shown in Table 2, are higher than the experimentally measured values for all but one combination of heat treatment and test temperature. This overprediction may be explained by the pre-existing manufacturing defects that exist in the composite, as discussed in section 2 and as Figs. 1, 3, 4 and 12 indicate, which dominate the inelastic deformation and result in large debonded areas and fiber/matrix separation under

applied loading. Such defects may unload the matrix substantially and therefore result in fewer numbers of cracks developed, and thus measured, in the microstructure.

4 SUMMARY

A SiC/Ti-15-3 MMC was studied to determine the effects of different heat treatments on the damage evolution at both room temperature and at 427°C. The thermomechanical study revealed that the heat treatments could affect the overall composite compliance and damage accumulation. Mechanical tests show that the 450°C heat treatment creates a microstructure with a consistently high elastic modulus and high damage tolerance for all loading conditions and temperatures.

Microstructural evaluation identified the primary damage modes for both the transverse and axial specimens. The axial specimens showed evidence of cracks developing perpendicular to the loading direction starting from the fiber/matrix interface. The transverse specimens showed cracks emanating from areas of poor consolidation resulting in cracks propagating in the loading direction along grain boundaries.

A model based on the Mori-Tanaka method was developed and implemented which combines both plasticity and damage in an incremental formulation. The developed method successfully simulates the stress vs. strain response of the composite accounting for both plastic deformation and damage. A prediction of the crack density was made as a function of overall applied load. It was shown that the predicted crack density at the final load level overpredicts the crack densities measured from a post-test microstructural analysis for the transverse specimens, most likely due to the pre-existing damage.

5 ACKNOWLEDGEMENTS

The authors acknowledge the support of AFOSR grant No. F49620-94-1-0341.

6 REFERENCES

Allen, D.H., Eggleston, M.R., and Hurtado, L.D., 1994, "Recent Research on Damage Development in SiC/Ti Continuous Fiber Metal Matrix Composites," in Fracture of Composites, E.A. Armanios, Ed., in *Key Engineering Materials* series, Trans Tech Publications.

Benveniste, Y., 1987, "A New Approach to the Application of the Mori-Tanaka's Theory in Composite Material," *Mech. Materials*, Vol. 6, pp.147-157.

Christensen, R.M., 1979, Mechanics of Composite Materials, Wiley Press, New York.

Dvorak, G.J., Laws, N., and Hejazi, M.,1985, "Analysis of Progressive Matrix Cracking in Composite Laminates I. Thermoelastic Properties of a Ply with Cracks," *J. Composite Mat.*, Vol. 19, pp. 216-234.

Foulk, J.W., Allen, D.H., and Lagoudas, D.C., "A Micromechanical Model for Predicting Fatigue Response of Metal Matrix Composites Subjected to Environmental Degradation," *Proc. IUTAM Symposium on Transformations in Composites*, Cairo, Egypt, 1997.

Gavazzi A.C., and Lagoudas, D.C. 1990, "Incremental Elastoplastic Behavior of Metal Matrix Composites Based on Averaging Schemes," *Proceedings IUTAM Symposium on Inelastic Deformation of Composite Materials*, G.J. Dvorak, ed. Springer-Verlag, pp. 465-485.

Hill, R., 1965, "Theory of Mechanical Properties of Fibre-Strengthened Materials: III. Self-Consistent Model," *J. Mechanics and Physics of Solids*, 13, pp.189-198.

Jeong, G.S., D.H. Allen, and D.C. Lagoudas, 1994, "Residual Stress Evolution due to Cool Down in Viscoplastic Metal Matrix Composites," *Int. J. Solids and Structures*, Vol.31, No. 19, pp. 2653-2677.

Johnson, W.S., 1992, NASA Technical Memorandum 107597, Lewis Research Center.

Johnson, W.S., S.J. Lubowinski and A.L. Highsmith, 1990, "Mechanical Characterization of Unnotched SCS-6/Ti-15-3 Metal Matrix Composites at Room Temperature," *Thermal and Mechanical Behavior of Metal Matrix and Ceramic Matrix Composites, ASTM STP 1080*, J.M. Kennedy et al., eds., ASTM, Philadelphia, PA, pp. 193-218.

Lagoudas, D.C., X. Ma, D.A. Miller and D.H. Allen, 1995, "Modeling of Oxidation in Metal Matrix Composites," *Int. J. Engng Sci.*, Vol. 33, No.15, pp. 2327-2343.

Lagoudas, D.C., Gavazzi, A.C., and Nigam, H., 1991,"Elastoplastic Behavior of Metal Matrix Composites Based on Incremental Plasticity and the Mori-Tanaka Averaging Scheme," *Computational Mechanics*, Vol. 8, pp. 283-308.

Laws, N., and Dvorak, G. J., 1987, “The Effect of Fiber Breaks and Aligned Penny-Shaped Cracks on the Stiffness and Energy Release Rates in Uni-directional Composites”, *Int. J. Solids and Structures*, Vol. 23, No.9, pp.1269-1283.

Lerch, B.A., Gabb, T.P., and MacKay, R.A., 1990a, "Heat Treatment Study of the SiC/Ti-15-3 Composite System," NASA TP 2970.

Lerch, B.A., Hull, D.R., and Leonhardt, T.A., 1990b, "Microstructure of a SiC/Ti-15-3 Composite," *Composites*, Vol. 21, No. 3, pp. 216-224.

Lerch, B.A. and Saltsman J.F., 1991, "Tensile Deformation Damage in SiC Reinforced Ti-15V-3Cr-3Al-3Sn," NASA Technical Memorandum 103620, Lewis Research Center.

Lissenden, Herakovich, C.T., Pindera, M.J., 1995a, “Response of SiC/Ti under Combined Loading part I: Theory and Experiment for Imperfect Bonding,” *Journal of Composite Materials*, Vol. 29 no. 2, pp. 130-155.

Lissenden, C.J., Herakovich, C.T., Pindera, M.J., 1995b, “Response of SiC/Ti under Combined Loading part II: Room Temperature Creep Effects ,” *Journal of Composite Materials*, Vol. 29 no. 10, pp. 1403-17.

Lissenden, C.J., Lerch, B.A., Herakovich, C.T., 1996, “Response of SiC/Ti under Combined Loading part III: Microstructural Evaluation,” *Journal of Composite Materials*, Vol. 30 no. 1, pp. 84-108.

Majumdar B.S. and G.M. Newaz, 1992a, NASA Contractor Report 189095, Lewis Research Center.

Majumdar B.S. and G.M. Newaz, 1992b, NASA Contractor Report 189096, Lewis Research Center.

Majumdar B.S. and G.M. Newaz, 1993, NASA Contractor Report 191181, Lewis Research Center.

Mori, T. And K. Tanaka, 1973, “Average Stress in Matrix and Average Elastic Energy of Materials with Misfitting Inclusions,” *Acta Metallurgica*, 21, pp. 571-574.

Mura, T., 1982, Micromechanics of Defects in Solids, Klewer Press, Boston.

Newaz G.M, Majumdar B.S, and F.W. Brust, 1992, “ Thermal Cycling Response of Quasi-Isotropic Metal Matrix Composites,” *J. Engineering Materials and Technology*, 114, pp. 156-161.

Okada, M., Banergee, D.,1984, "Tensile Properties of Ti-15V-3Al-3Cr-3Sn Alloy," *Titanium Science and Technology: Proceedings of the Fifth International Conference on Titanium*, Munich, Germany, Luetjering ed., Deutsch Gesellschaft fur Metallkunde, Pub., pp.1835-1842.

Sun, C.T., J.L. Chen, G.T. Sha, and W.E. Koop. 1990. "Mechanical Characterization of SCS-6/Ti-6-4 Metal Matrix Composite," *J. Composite Mat.*, Vol. 24, pp. 1029-1059.

Weng, G.J., 1984, “Some Elastic Properties of Reinforced Solids, with Special Reference to Isotropic ones Containing Spherical Inclusions”, *Int. J. Ingrg Sci*., Vol. 22, pp.845-856.

Wolfenden, A., K.D. Hall, and B.A. Lerch, 1996, “The effect of heat treatment on Young’s modulus, damping, and microhardness of SiC/Ti-15-3,” *J. of Materials Science*, Vol. 31, pp. 1489-1493.

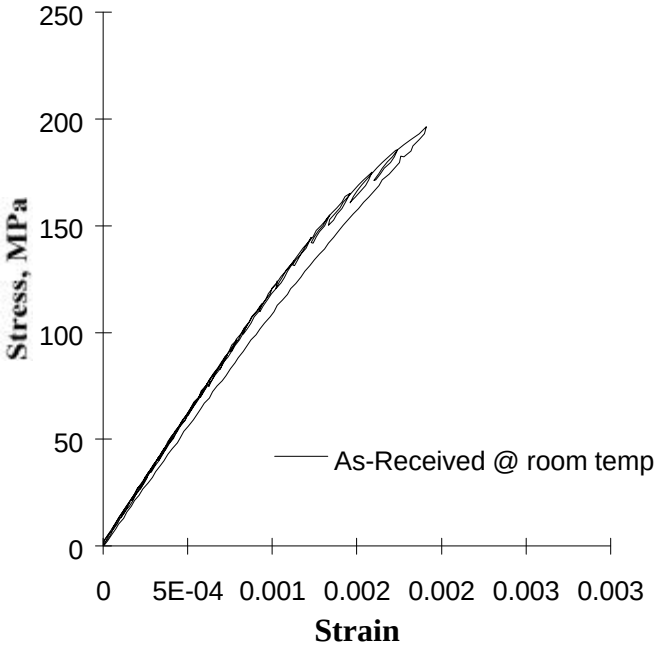
250
200
150
100
50
0
Stress, MPa
As-Received @ room temp
0
5E-04
0.001
0.002
0.002
0.003
0.003
Strain

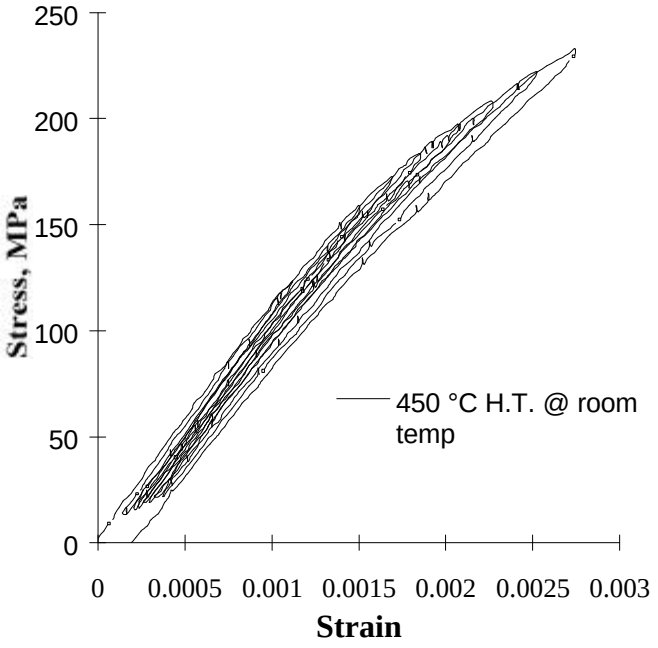
250
200
150
100
50
0
Stress, MPa
450 °C H.T. @ room temp
0
0.0005
0.001
0.0015
0.002
0.0025
0.003
Strain

a.) b.)

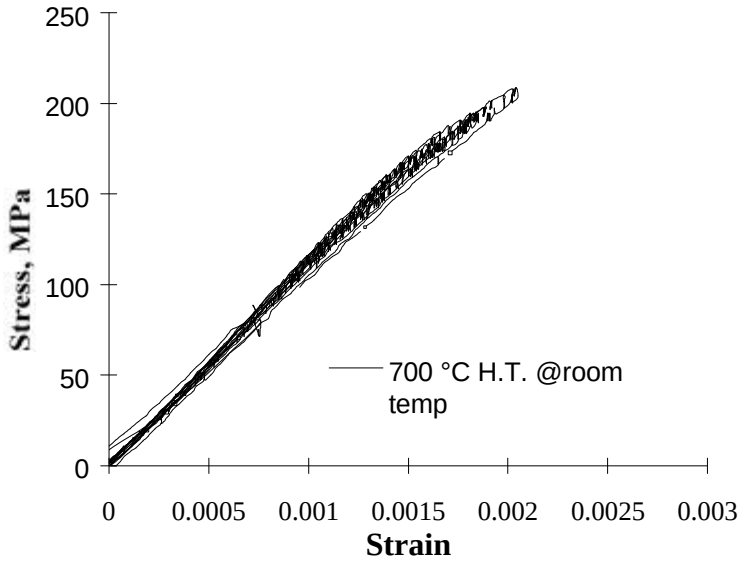

c.)

Fig. 9 Stress vs. Strain for $[90]_4$ specimens tested at room temperature for a.) as-received, b.) 450 °C

heat treatment and c.) 700 °C heat treatment.

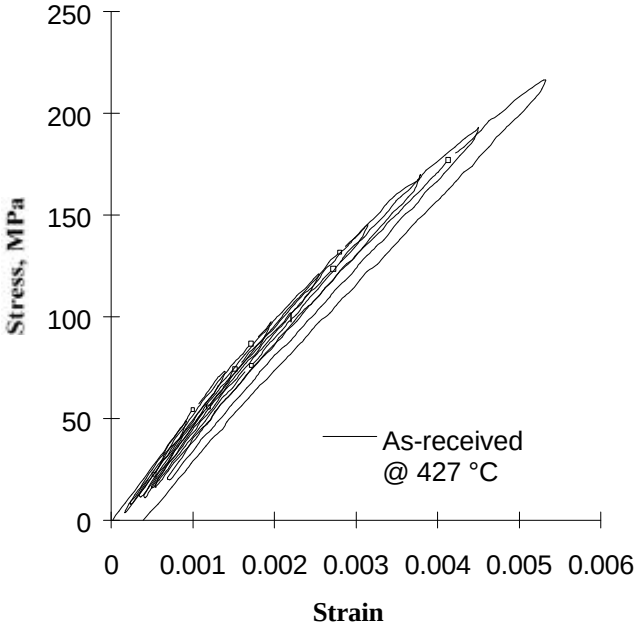
250
200
150
100
50
0
Stress, MPa
As-received
@ 427 °C
0
0.001
0.002
0.003
0.004
0.005
0.006
Strain

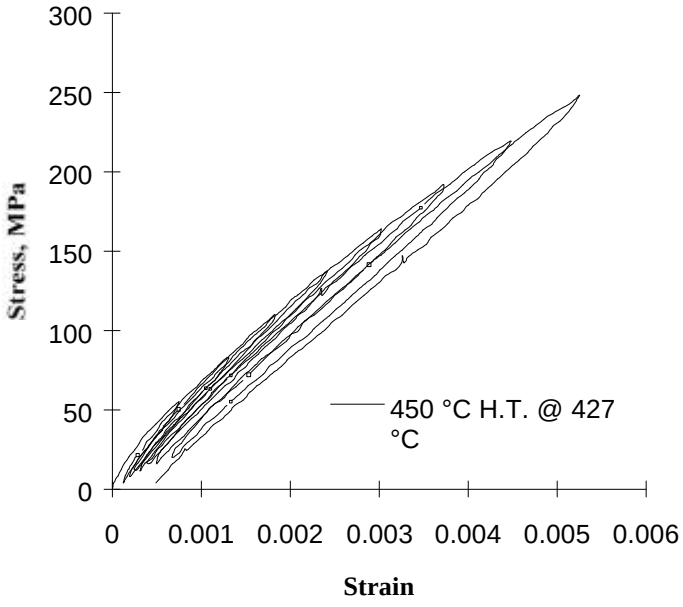
300
250
200
150
100
50
0
Stress, MPa
450 °C H.T. @ 427
°C
0
0.001
0.002
0.003
0.004
0.005
0.006
Strain

a.)

b.)

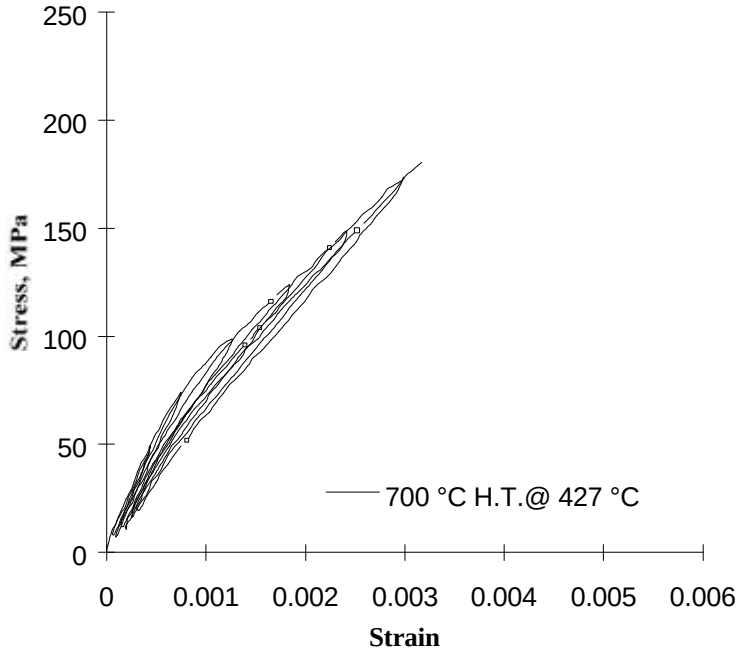

c.)

Fig. 10 Stress vs. Strain for $[90]_4$ specimens tested at 427 °C for a.) as-received, b.) 450 °C heat treatment and c.) 700 °C heat treatment.

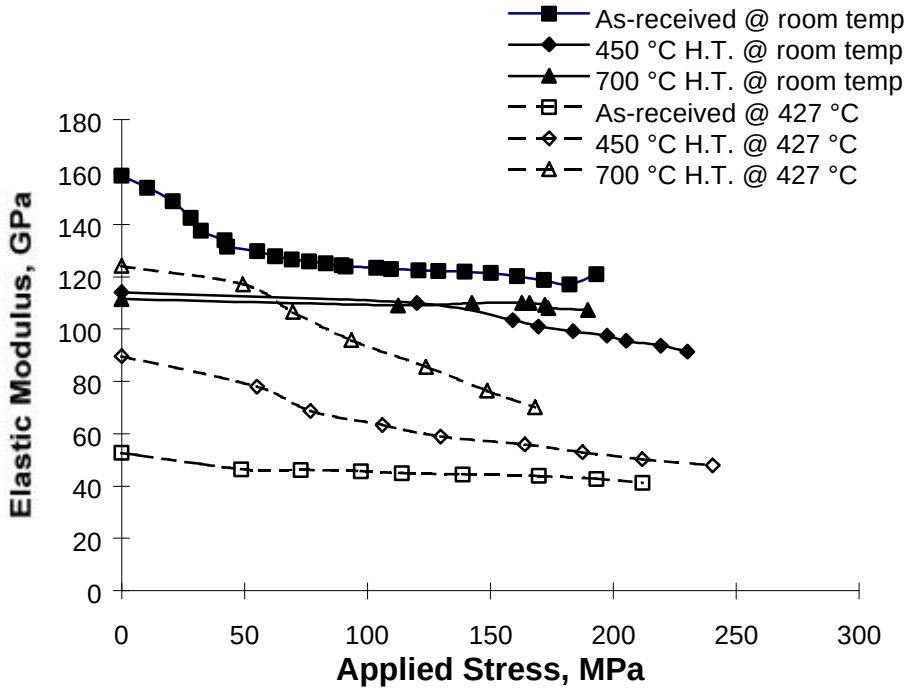

Fig. 11 Unloading Elastic Modulus vs. Applied Stress for transverse specimens.

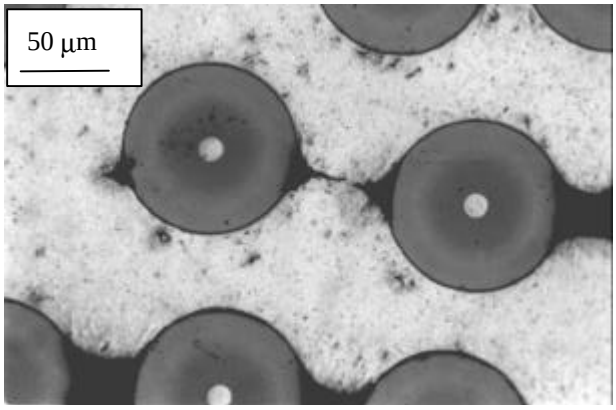

a.)

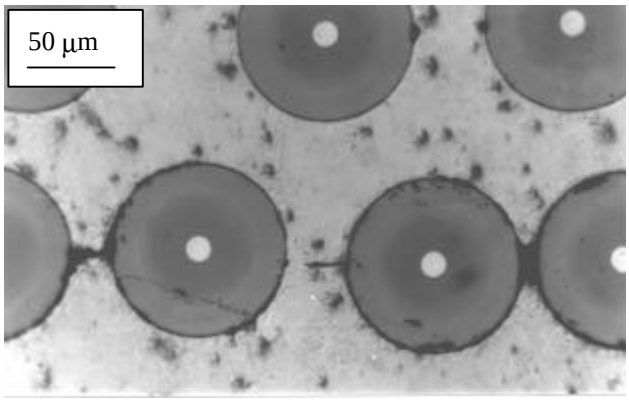

b.)

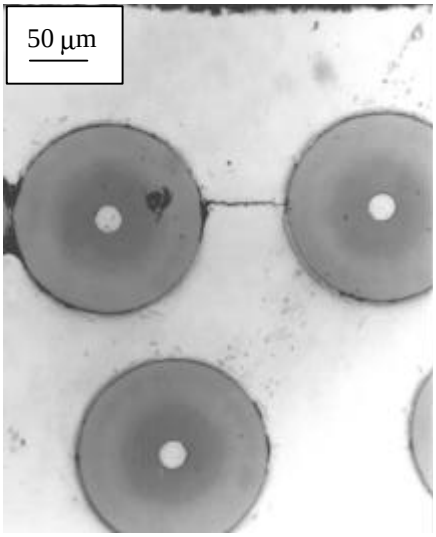

c.)

Fig. 12 Cracks seen in transverse specimens showing crack propagation in un-etched specimens for a.) as-received, b.) 450 °C heat treatment and c.) 700 °C heat treatment.

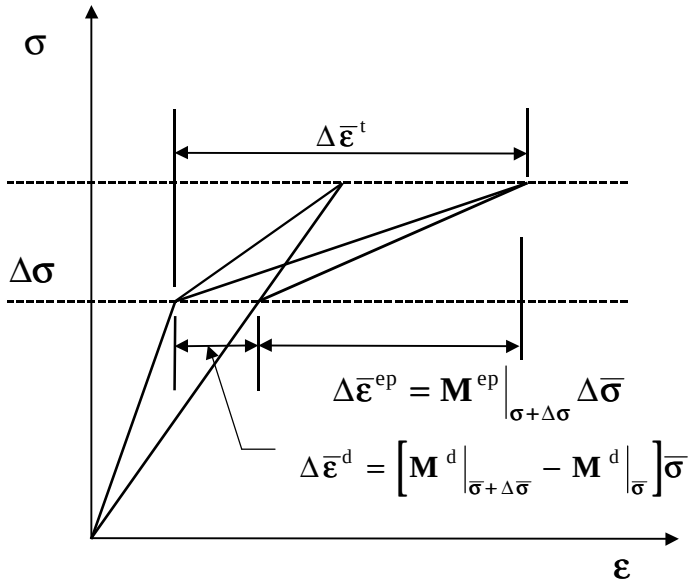

Fig. 13 Schematic representation of uni-axial loading path showing damage and plastic strain increments over loading increment, $\Delta\boldsymbol{\sigma}$.

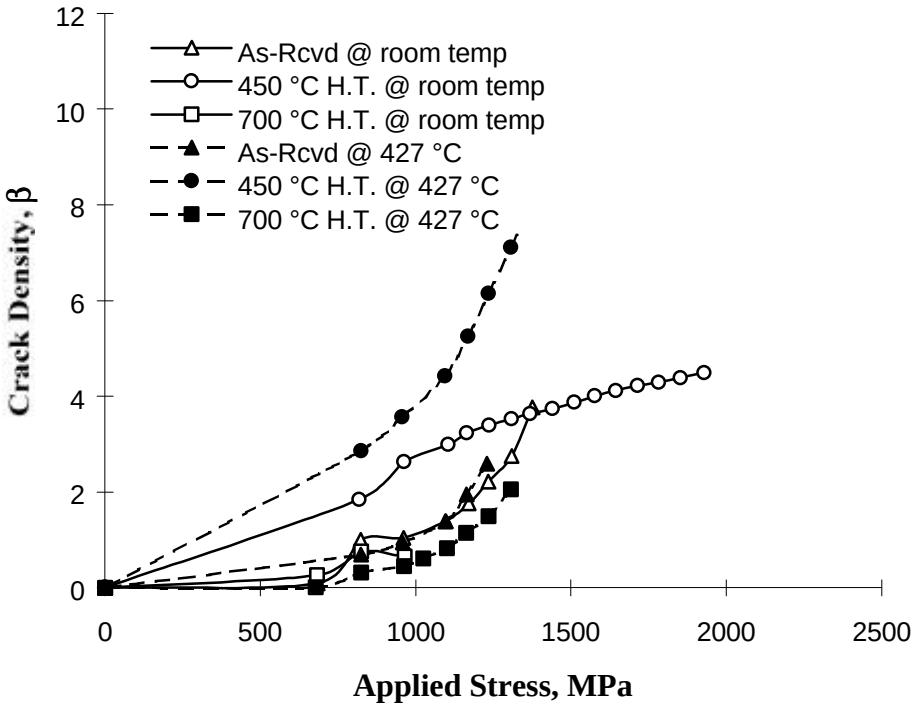
12
10
8
6
4
2
0
Crack Density, β
As-Rcvd @ room temp
450 °C H.T. @ room temp
700 °C H.T. @ room temp
As-Rcvd @ 427 °C
450 °C H.T. @ 427 °C
700 °C H.T. @ 427 °C
0
500
1000
1500
2000
2500
Applied Stress, MPa

a.)

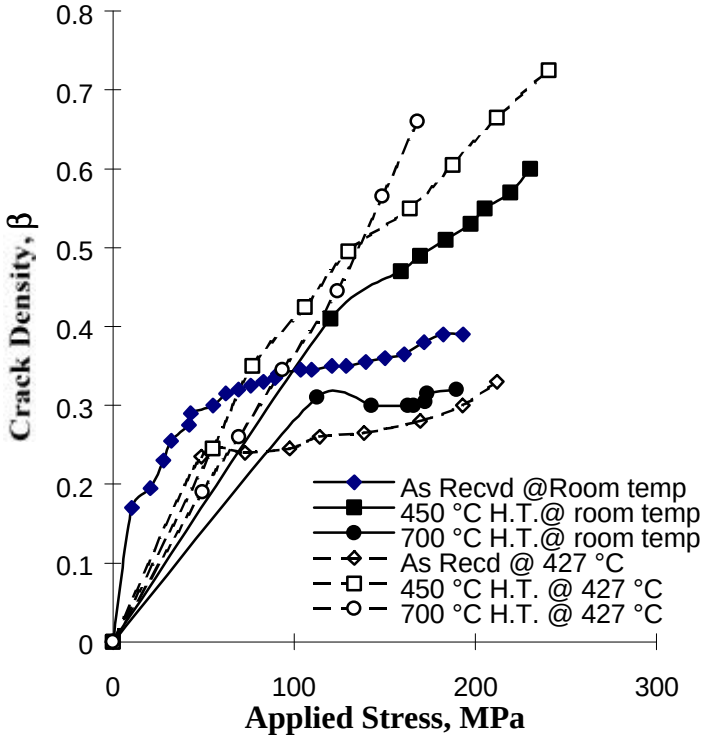

b.)

Fig. 14 Prediction of crack density as a function of load for a.) axial crack density, $\beta^{a.}$ and b.) transverse crack density, β^{tr}.

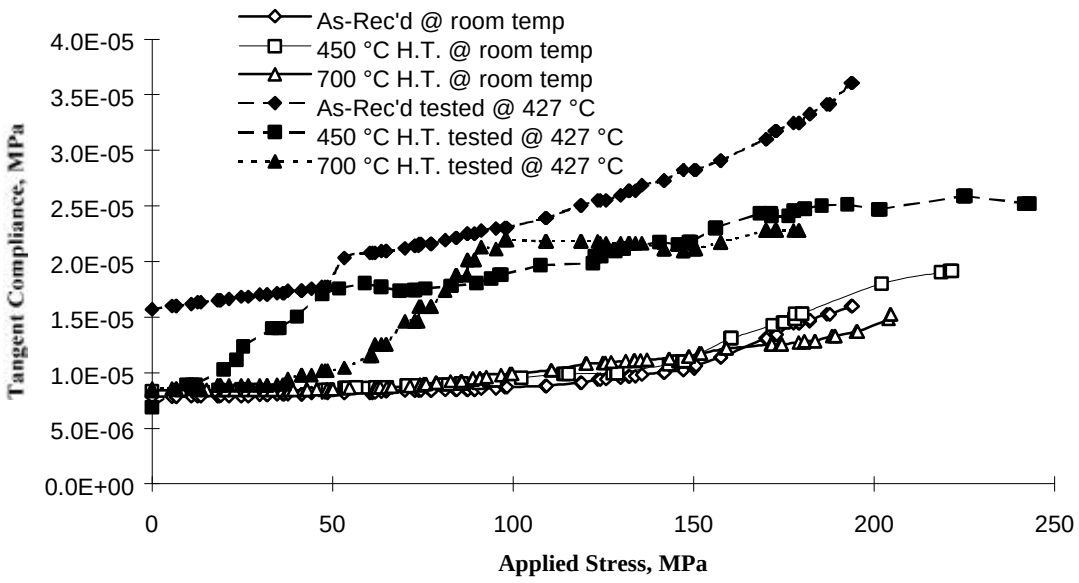

Fig. 15 Instantaneous plastic compliance vs. applied stress for simulation of plastic stress/strain evolution.

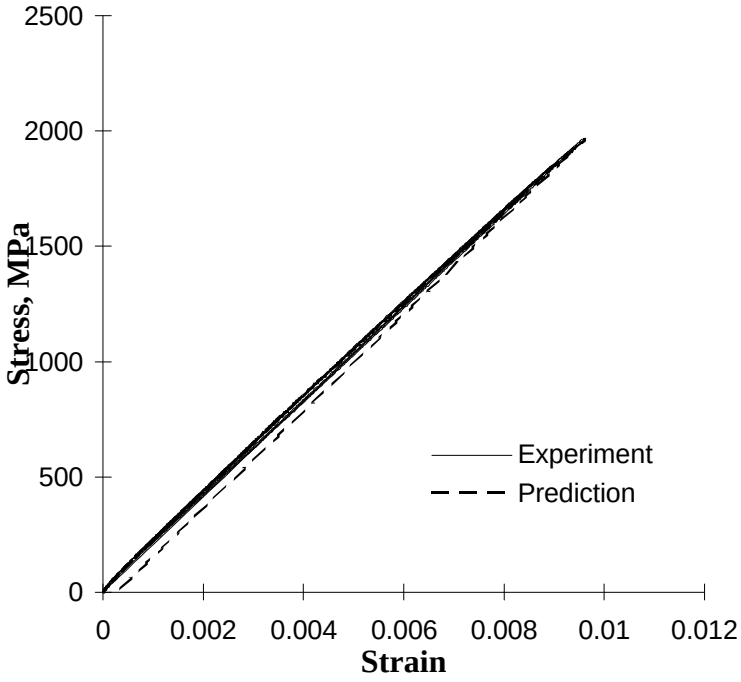
2500
2000
1500
1000
500
0
Stress, MPa
0
0.002
0.004
0.006
0.008
0.01
0.012
Strain
Experiment
Prediction

a.)

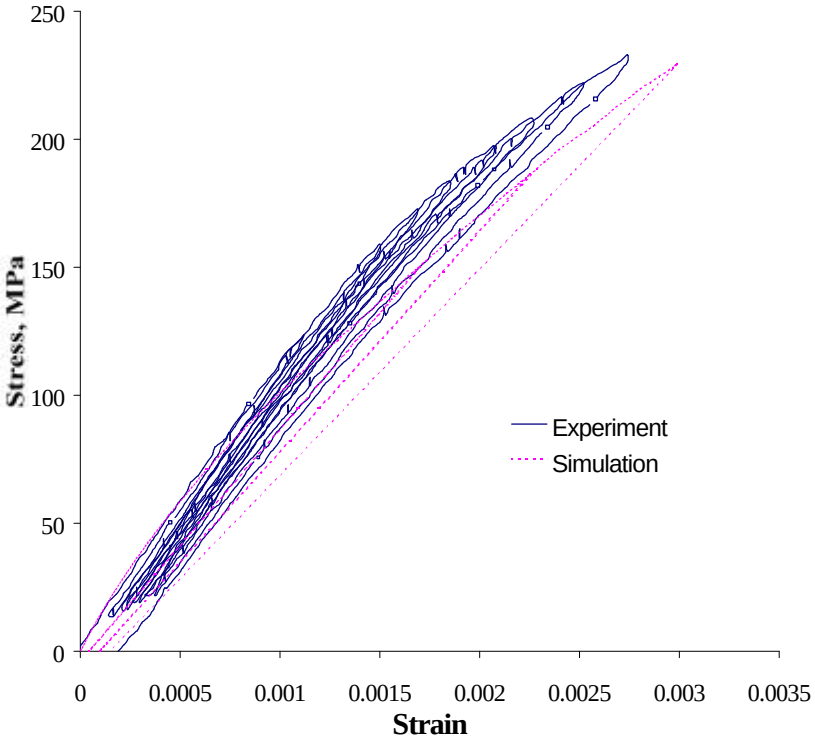
250
200
150
100
50
0
Stress, MPa
0
0.0005
0.001
0.0015
0.002
0.0025
0.003
0.0035
Strain
Experiment
Simulation

b.)

Fig. 16. Simulated Stress vs. Strain response combining plasticity and damage effects plotted with experimental results for uni-directional a.) axial composite and b.) transverse composite.